J. Geophys. 48, 84–93, 1980

Journal of Geophysics

The Simulation Problem for Broad-Band Seismograms

D. Seidl

Seismologisches Zentralobservatorium Graefenberg, Krankenhausstr. 1–3, D-8520 Erlangen, Federal Republic of Germany

Abstract. A fundamental problem in the numerical data pre-processing of digital broad-band seismograms is the simulation of arbitrary analog seismograph systems, especially seismometer-galvanometer combinations. A special case of this simulation problem is the deconvolution or restitution problem as the realization of a wide-band seismograph system with a transfer function proportional to ground displacement, velocity or acceleration. The simulation problem can be solved by a digital cascade recursive filter using the bilinear z-transformation. Applications of the simulation filter are: a combined interpretation of digital broad-band and analog narrow-band recordings, a routine analysis of broad-band seismograms consistent with ordinary analog stations, the determination of the local magnitude from simulated Wood-Anderson seismograms and the restitution of broad-band recordings. The relationship between bandwidth, fine structure and information content of seismograms can be demonstrated in an obvious way by comparing broad-band recordings of the Graefenberg-array with simulated seismograms for different standardized seismometer-galvanometer systems.

Key words: Graefenberg-array – Broad-band seismograms – Simulation and restitution problem – Bandwidth and fine structure of seismograms.

Introduction

A fundamental problem in the pre-processing of digital broad-band seismograms is the simulation of arbitrary band-limited seismograph systems. A special case of this simulation problem is the restitution problem as a realization of a seismograph system whose transfer function is directly proportional to ground displacement, velocity or acceleration in the broadest possible frequency range.

While the application of simple band-pass filters is sufficient for routine analysis of broad-band seismograms (determination of arrival time, body wave magnitude, surface wave magnitude, etc.), for simultaneous processing of digital broad-band recordings and analog narrow-band seismograms it often proves necessary or desirable to have the most exact possible simulation of the corresponding analog seismograph system. The analysis of the Bukarest earthquake on March 4, 1977, is an instructive practical example of this simulation problem (Müller et al. 1978).

Data for the realization of the simulation problem are digital broad-band seismograms from the 3-component station A1 (A1-Z, A1-N, A1-E) of the Graefenberg subarray A. The recording is proportional to ground velocity between the 3-db frequencies 0.05 Hz (seismometer) and 5 Hz (anti-aliasing filter). The dynamic range of the final version of the data acquisition system is 132 db (not 138 db as it was intended; Harjes and Seidl 1978), the resolution is 66 db. Due to the large dynamic range and high resolution, as well as the small low-frequency noise level of the feedback leaf-spring seismometer STS-1V and STS-1H (Wielandt 1973, 1975; Streckeisen 1978) it is possible to vary the shape and bandwidth of the transfer function by digital methods to a large degree.

Simulation of Seismometer-Galvanometer Systems

Seismometer-galvanometer combinations are the most important narrow-band seismograph systems. A summary and classification of the standardized response functions is included in the Manual of Seismological Observatory Practice (Willmore and Karnik 1970). Figure 1 shows the amplitude response to ground displacement for the WWSSN-LP, WWSSN-SP, GALITZIN and KIRNOS system. The appropriate instrument parameters T_1, h_1, T_2, h_2 (natural period and damping constant of seismometer and galvanometer), as well as the period at maximum (T_{max}) and the periods at the 3-db points of the amplitude response (T_l, T_u) are summarized in Table 1.

An exact simulation of the WWSSN-SP system would require the incorporation of the inductive coil reactances of the seismometer (BENIOFF-seismometer of the variable reluctance type) and the galvanometer (Savill et al. 1962; Chakrabarty et al. 1964). For the practical processing of seismograms (determination of arrival time and body wave magnitude, improvement of signal-to-noise ratio) an approximation using a suitable induction free system is sufficient. As an example, Fig. 1 shows the amplitude response of a seismometer-galvanometer combination ($T_1=1.05$ s, $h_1=0.67$, $T_2=0.75$ s, $h_2=0.55$) which is a very good approximation of the magnification curve between 0.1 and 5.0 Hz for the WWSSN-station Stuttgart.

Neglecting the galvanometer coupling factor and omitting constant amplitude factors, the transfer function of the simulation filter $H_{SG}(s)$ which transforms the broad-band seismogram u into the simulated seismogram w is given by

$$H_{SG}(s)=H_0^{-1}(s)\cdot H_1(s)\cdot H_2(s). \tag{1}$$

$$H_0^{-1}(s)=\frac{s^2+2h_0\omega_0 s+\omega_0^2}{s^3} \tag{2}$$

0340-062X/80/0048/0084/$02.00

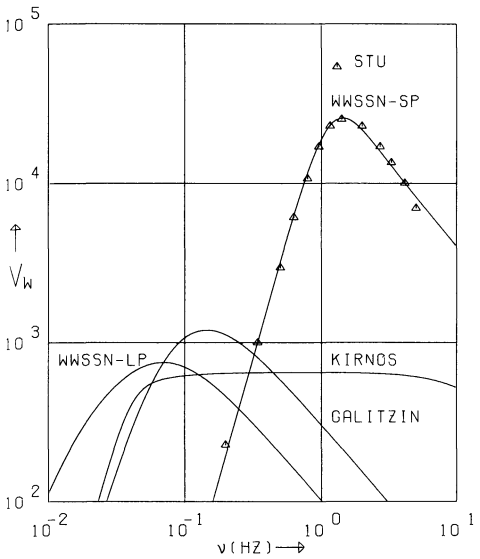

Fig. 1. Magnification curves of the seismometer-galvanometer systems WWSSN-SP, WWSSN-LP, GALITZIN and KIRNOS. Instrument parameters in Table 1. Δ measured magnifications of WWSSN-SP station Stuttgart (STU)

is the inverse transfer function of the broad-band seismometer (velocity transducer with the natural period $T_0=2\pi/\omega_0$ and damping constant h_0),

$$H_1(s)=\frac{s^3}{s^2+2h_1\omega_1 s+\omega_1^2} \tag{3}$$

is the transfer function of the simulated seismometer (velocity transducer with the natural period $T_1=2\pi/\omega_1$ and damping constant h_1), and

$$H_2(s)=\frac{\omega_2^2}{s^2+2h_2\omega_2 s+\omega_2^2} \tag{4}$$

is the transfer function of the simulated galvanometer (natural period $T_2=2\pi/\omega_2$, damping constant h_2).

Combining Eqs. (1) to (4) gives

$$H_{SG}(s)=H_E(s)\cdot H_G(s)=\frac{s^2+2h_0\omega_0 s+\omega_0^2}{s^2+2h_1\omega_1 s+\omega_1^2}\cdot\frac{\omega_2^2}{s^2+2h_2\omega_2 s+\omega_2^2}. \tag{5}$$

The first factor $H_E(s)$ in Eq. (5) is the transfer function of an inverse filtering circuit as described by Wielandt (1970). The second factor $H_G(s)$ corresponds to the low-pass characteristic of the galvanometer or a corresponding electronic filter (Wielandt and Mitronovas 1976).

Since $H_{SG}(s)$ in Eq. (5) takes the form of the product of two polynomial fractions in s, it is obvious that simulation can be approximated by a cascade of two recursion filters in the time domain (Beauchamp 1973). The transition from the s-plane of the continuous system to the z-plane of a sampled-data filter with the digitization interval Δt can be made with the standard z-transform or the bilinear z-transformation (Kaiser 1963). The second, so-called z-form method has the advantage that no aliasing problems occur. On the other hand, it has the disadvantage that the entire imaginary frequency axis of the s-plane is mapped onto the unit circle of the z-plane, producing a non-linear distortion of the frequency scale. If the transfer function $H(s)$ can be pieced together from pass- and rejection-bands with approximately constant slopes, then the frequency distortion can be compensated for by a prewarping of the corner frequencies ω_i $(i=0, 1, 2)$ of the continuous system to $\bar{\omega}_i$ according to the conversion formula (Kaiser 1963; Beauchamp 1973)

$$\bar{\omega}_i=\frac{2}{\Delta t}\cdot\tan\frac{\Delta t\cdot\omega_i}{2}=\frac{2}{\Delta t}\omega_i'. \tag{6}$$

The bilinear z-transformation

$$s=\frac{2}{\Delta t}\cdot\frac{z-1}{z+1} \tag{7}$$

then shifts the prewarped values $\bar{\omega}_i$ to the desired values ω_i.

Substituting ω_i for $\bar{\omega}_i$ after Eq. (6) and inserting Eq. (7) into Eq. (5) the z-transform $H_E^*(z)$ of the inverse filter factor becomes

$$H_E^*(z)=\frac{V^*(z)}{U^*(z)}=\frac{\left(\frac{z-1}{z+1}\right)^2+k_0'\frac{z-1}{z+1}+\omega_0'^2}{\left(\frac{z-1}{z+1}\right)^2+k_1'\frac{z-1}{z+1}+\omega_1'^2}=\frac{a_0+a_1z^{-1}+a_2z^{-2}}{1+b_1z^{-1}+b_2z^{-2}} \tag{8}$$

where $\omega_i'=\tan(\Delta t\cdot\omega_i/2)$ after Eq. (6) and $k_i'=2h_i\omega_i'$ $(i=0, 1)$.

$V^*(z)$ and $U^*(z)$ are the z-transforms of the inverse filter output v_t and of the broad-band seismogram u_t respectively.

The filter coefficients in Eq. (8) are given by

Table 1. Parameters of standardized seismometer-galvanometer systems

	T_1 (s)	h_1	T_2 (s)	h_2	T_l (s)	T_{max} (s)	T_u (s)
WWSSN-LP (V_w)	15.0	1.0	100.0	1.0	6.06	14.40	32.29
WWSSN-SP (V_w)	1.05	0.67	0.75	0.55	0.42	0.69	1.02
GALITZIN (V_w)	12.0	1.0	12.0	1.0	3.15	6.93	12.98
KIRNOS (V_w)	25.0	0.5	1.2	8.0	0.08	1.45	22.47
BENIOFF-LP (V_G)	1.0	0.5	100.0	0.5	0.87	70.75	116.9

T_1, T_2: Natural period of seismometer resp. galvanometer
h_1, h_2: Damping constant of seismometer resp. galvanometer
T_{max}, T_l, T_u: Maximum period, lower and upper 3-db period of magnification curve for ground displacement (V_w) resp. ground velocity (V_G) in Fig. 1

$$a_0=\frac{1}{b_0}(\omega_0'^2+k_0'+1)$$

$$a_1=\frac{2}{b_0}(\omega_0'^2-1)$$

$$a_2=\frac{1}{b_0}(\omega_0'^2-k_0'+1)$$

$$b_1=\frac{2}{b_0}(\omega_1'^2-1)$$

$$b_2=\frac{1}{b_0}(\omega_1'^2-k_1'+1) \tag{9}$$

with

$$b_0=\omega_1'^2+k_1'+1.$$

Correspondingly, the z-transform of the galvanometer factor $H_G^*(z)$ in Eq. (5) becomes

$$H_G^*(z)=\frac{W^*(z)}{V^*(z)}=\frac{\omega_2'^2}{\left(\frac{z-1}{z+1}\right)^2+k_2'\frac{z-1}{z+1}+\omega_2'^2}$$

$$=\frac{c_0(1+2z^{-1}+z^{-2})}{1+d_1z^{-1}+d_2z^{-2}} \tag{10}$$

where $\omega_2'=\tan(\Delta t\cdot\omega_2/2)$ after Eq. (6) and $k_2'=2h_2\omega_2'$.

$W^*(z)$ is the z-transform of the simulated seismogram w_t. The filter coefficients in Eq. (10) are

$$c_0=\frac{1}{d_0}\omega_2'^2$$

$$d_1=\frac{2}{d_0}(\omega_2'^2-1)$$

$$d_2=\frac{1}{d_0}(\omega_2'^2-k_2'+1) \tag{11}$$

with

$$d_0=\omega_2'^2+k_2'+1.$$

Rearranging Eqs. (8) and (10) gives

$$V^*(z)\cdot(1+b_1z^{-1}+b_2z^{-2})=U^*(z)\cdot(a_0+a_1z^{-1}+a_2z^{-2}) \tag{12}$$

$$W^*(z)\cdot(1+d_1z^{-1}+d_2z^{-2})=V^*(z)\cdot c_0(1+2z^{-1}+z^{-2}). \tag{13}$$

Application of the shifting theorem

$$X^*(z)\cdot z^{-k}\equiv x_{t-k} \tag{14}$$

converts Eqs. (12) and (13) into difference equations:

$$v_t=a_0u_t+a_1u_{t-1}+a_2u_{t-2}-b_1v_{t-1}-b_2v_{t-2} \tag{15}$$

$$w_t=c_0(v_t+2v_{t-1}+v_{t-2})-d_1w_{t-1}-d_2w_{t-2}. \tag{16}$$

Eqs. (15) and (16) describe a two-step recursion filter which transforms the broad-band seismogram u_t into the simulated seismogram w_t. The output of the first step corresponds to the output of a seismometer with natural period $T_1=2\pi/\omega_1$ (digital inverse filtering). The upper cut-off frequency of w_t is determined by the anti-aliasing filter of the data acquisition system (corner-frequency 5.0 Hz, slope 42 db/octave). Simulation of long period systems is best accomplished by data reduction with a low-pass filter followed by decimation. The z-form method can also be applied to the simulation of the SRO-system resulting in a seven-step recursion filter for the long-period channel. A detailed description will be given in a subsequent paper.

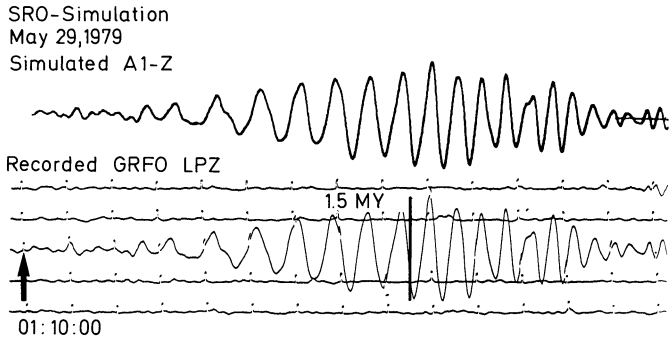

Fig. 2. Analog seismogram recorded by the LPZ-channel of the SRO-station GRFO and corresponding seismogram simulated from digital broad-band data of array station A1-Z. The horizontal distance between the stations is about 30 m, the vertical distance about 110 m

The simulation filter approximates the amplitude characteristic of the simulated system. The accuracy of the filter can be demonstrated most clearly by comparing simulated with recorded seismograms. Figure 2 shows an example for the long-period SRO-system. An example for a seismometer-galvanometer combination was given by Harjes and Seidl (1978). The most important applications of simulation filters are the simultaneous analysis of narrow-band and broad-band seismograms, routine processing compatible with analog stations, the approximate solution of the restitution problem, determination of local magnitude with simulated Wood-Anderson seismograms, as well as investigation of the dependence of the fine structure of seismograms as a function of the band-width and dynamic range of the seismograph system.

Broad-band seismograms contain a pronounced fine structure in the spectral range between 2 s and 20 s that is suppressed to a great extent by both the narrow-band analog stations and the new SRO-stations (Peterson et al. 1976). The main purpose of the Graefenberg-array is to record this fine structure in the frequency-wave number space with large dynamic range and high resolution. The broad-band seismograms in Figs. 3–11 are recordings of the 3-component station A1 of subarray A. Comparison between these broad-band recordings and the simulated seismograms of narrow-band systems makes it possible to demonstrate the relationship between fine structure or information content, band-width and dynamic range. The first example is given in Fig. 3. It shows the seismograms of the *P*-wave group from an Uzbekistan earthquake on May 7, 1976, for a broad-band recording BB-G proportional to ground velocity as well as the simulated seismograms for the WWSSN-LP and WWSSN-SP systems. The seismograms, which were calculated with a recursion filter, can also be visualized as the convolution of the broad-band seismogram with the velocity impulse response function of the seismometer-galvanometer system. The pulse-width of this function for the WWSSN-LP system is about 7 s. Fine structures that have a smaller time constant are smeared by convolution. The *P*-wave group in Fig. 3 consists of two signals which are 6 s apart. They appear in the WWSSN-LP seismogram only as a broadening of the impuls and are lost to direct interpretation (pP-phase of double shock). Only the arrival time

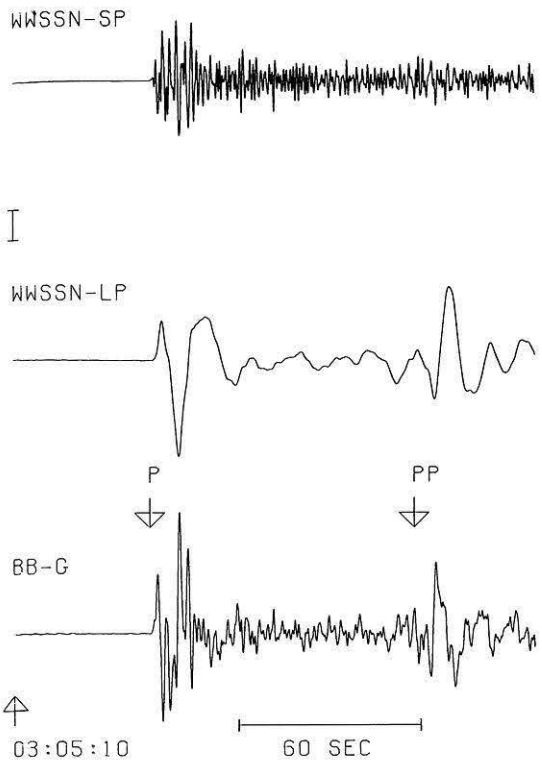

and the spectral amplitude in the frequency band around 1 Hz can be read from the amplitude modulated, quasi-monochromatic WWSSN-SP seismogram.

Figure 4 shows the total broad-band recording BB-G as well as the simulated seismograms for the KIRNOS, GALITZIN and WWSSN-LP systems and demonstrates the superiority of the WWSSN-LP system for recording long-period surface waves.

Figures 5 and 6 show seismograms corresponding to those shown in Figs. 3 and 4, taken from the Bukarest earthquake on March 4, 1977. The *P*-wave group of the broad-band seismogram BB-G (Fig. 5) is made up of at least three impulses, whose separation in time is less than the width of the impulse response of the WWSSN-LP system, so that the individual impulses only appear as shoulders in the simulated WWSSN-LP seismogram. By comparing the BB-G and WWSSN-LP seismograms in Fig. 5 Müller et al. (1978) identified and correlated corresponding shoulders in the recordings of many WWSSN-stations and were

Fig. 3. Broad-band recording BB-G (proportional to ground velocity, upper 3-db period $T_u = 30$ s; $V_G = 10.4$ μ/s) and simulated seismograms of WWSSN-LP ($V_{max} = 750$) and WWSSN-SP ($V_{max} = 25{,}000$) system of an Uzbekistan earthquake (May 17, 1976, 02 h 58 m 40.6 s, 40.4 °N, 63.5 °E, $m_b = 6.3$, $\Delta = 37.4°$). Magnification V_G is related to marked amplitude scale, maximum magnification V_{max} to 1 cm

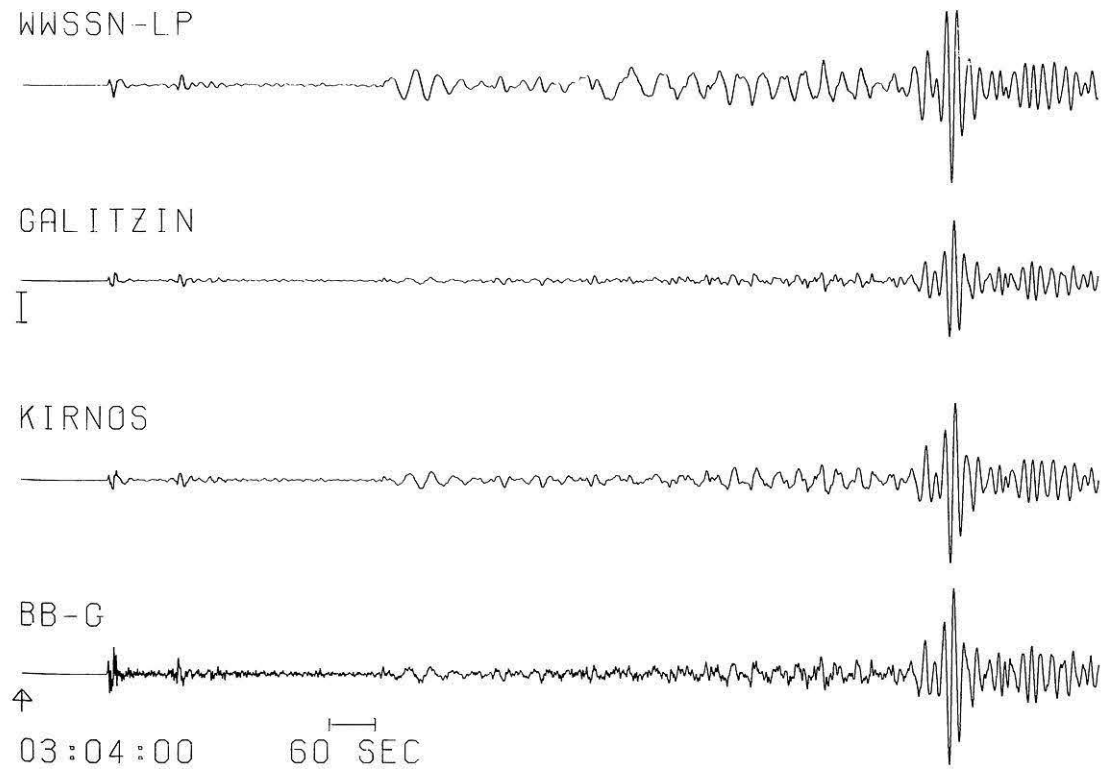

Fig. 4. Broad-band recording BB-G (proportional to ground velocity, $T_u = 30$ s; $V_G = 42$ μ/s) and simulated seismograms of KIRNOS, GALITZIN, and WWSSN-LP system ($V_{max} = 100$) for the same earthquake as in Fig. 3. Instrument parameters in Table 1

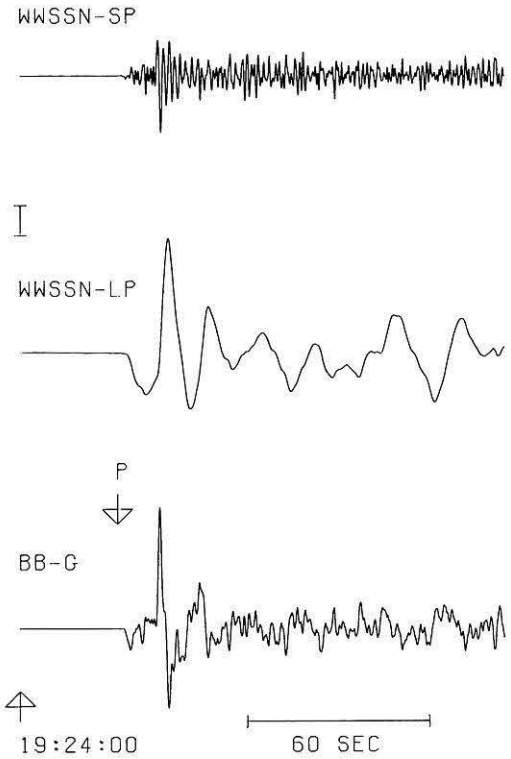

Fig. 5. Broad-band recording BB-G (proportional to ground velocity, $T_u = 30$ s, $V_G = 138$ μ/s) and simulated seismograms of WWSSN-LP ($V_{max} = 60$) and WWSSN-SP ($V_{max} = 2{,}500$) system of the Bukarest earthquake (March 4, 1977, 19 h 21 m 54.1 s, 45.8 °N, 26.8 °E, $m_b = 6.4$, $\Delta = 11.2°$)

thus able to show that the Bukarest earthquake was a multiple-shock.

Figure 7 shows a summary of simulated broad-band and narrow-band seismograms for a deep focus earthquake in the North Korea region on March 9, 1977. The *P*-wave group in the broad-band recording BB-G is made up of a low-frequency signal and a high-frequency phase arriving shortly after the first onset. The WWSSN-seismograms separate these two wave groups and contain in this example unlike to Fig. 3 and Fig. 5 the same information as the broad-band recording BB-G.

The seismograms in Figs. 3–7 demonstrate clearly the relationship between bandwidth, signalshape and information content. The narrow-band seismograms are more or less smooth whereas the broad-band recordings show a pronounced fine structure (for example multi-pulse signals, variation of amplitude and frequency with time) which cannot be completely reconstructed from digitized analog seismograms by deconvolution. The interpretation and inversion of this fine structure is the main object of broad-band seismology. Some examples should be mentioned: Phase identification and determination of source depth with theoretical seismograms (Kind 1979), determination of source parameters by spectral analysis (Stoll 1979) and by using the broad-band data as reference seismograms for the interpretation of analog recordings (Müller et al. 1978).

Simulation of a Wood-Anderson Seismograph

The local magnitude M_L is related to the maximum amplitude of a seismogram recorded on a Wood-Anderson seismograph. The usual practice of deriving M_L from some other kinds of

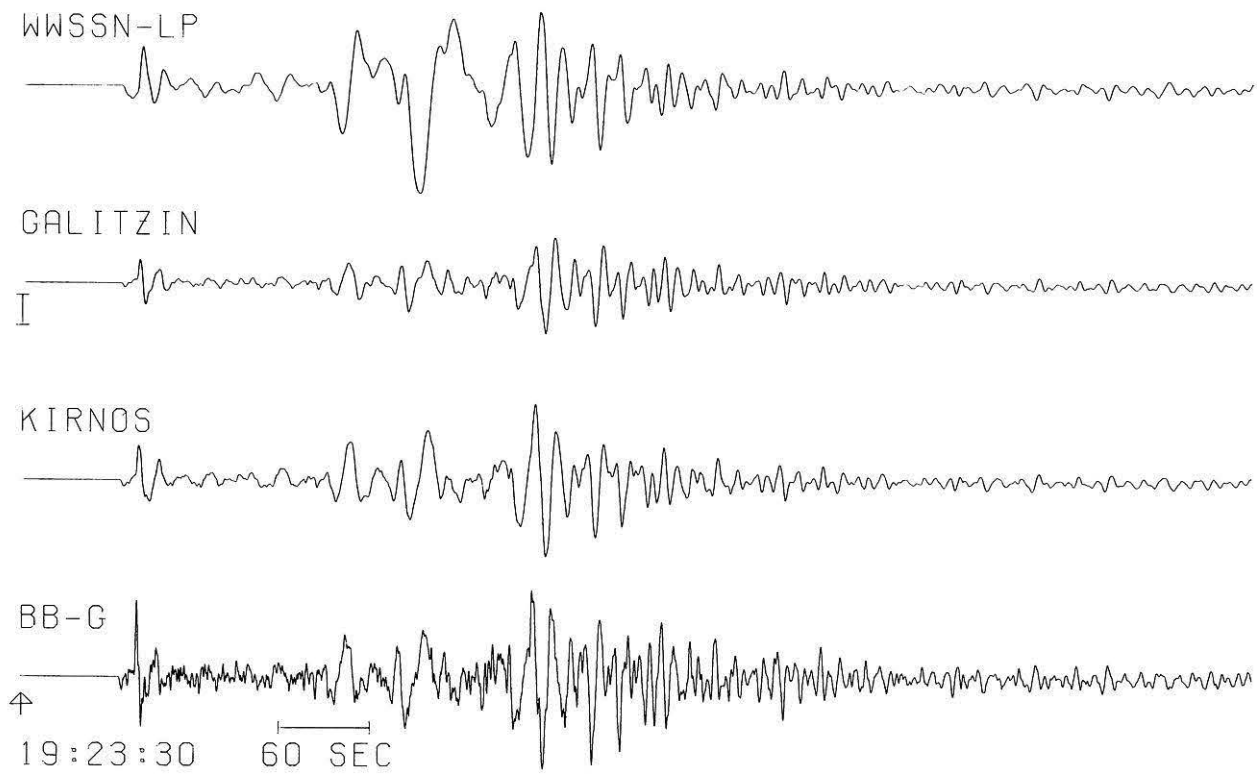

Fig. 6. Broad-band recording BB-G (proportional to ground velocity, $T_u = 30$ s, $V_G = 219$ μ/s) and simulated seismograms of KIRNOS, GALITZIN, and WWSSN-LP system ($V_{max} = 20$) for the same earthquake as in Fig. 5. Instrument parameters in Table 1

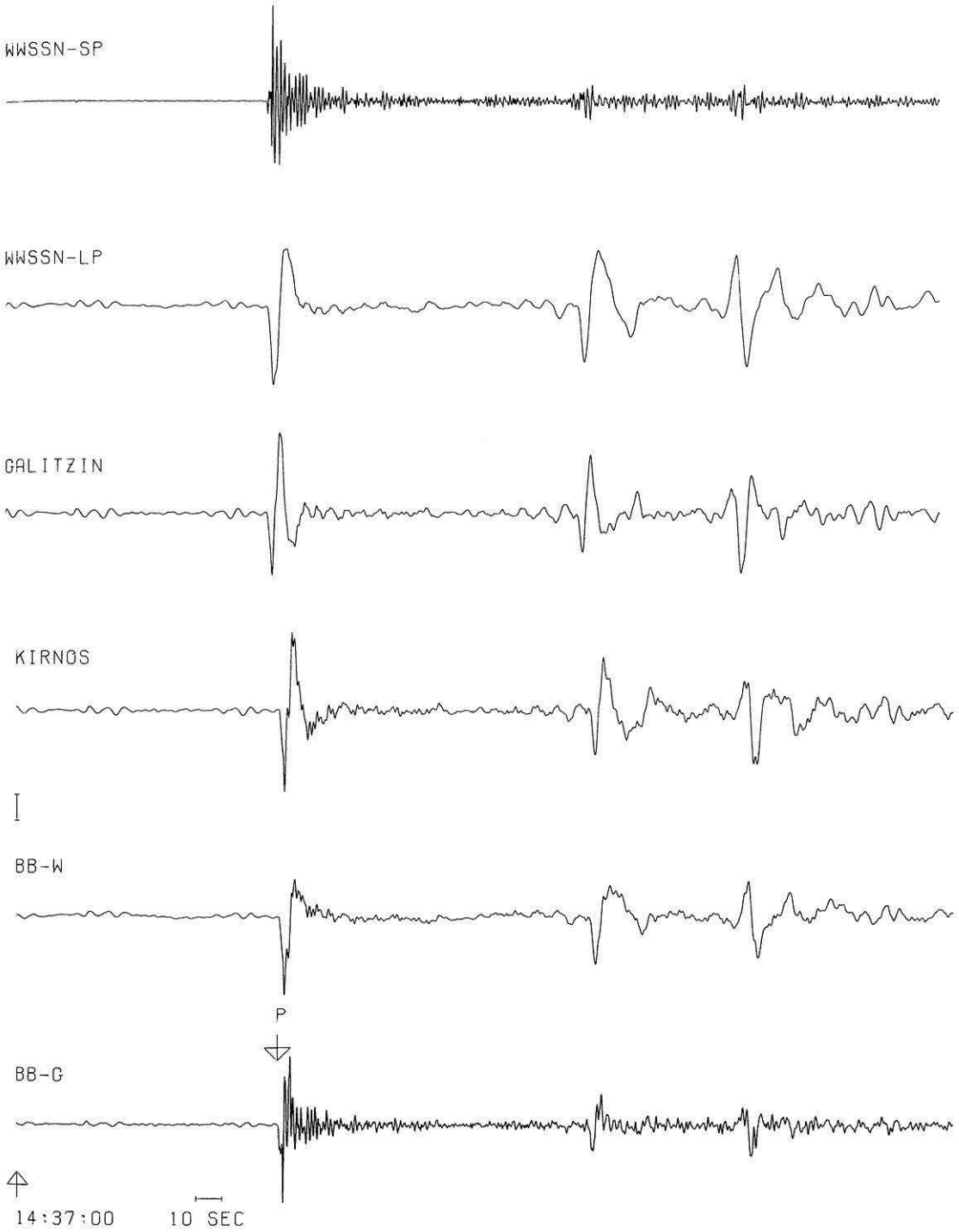

Fig. 7. Broad-band recording BB-G (proportional to ground velocity, $T_u = 100$ s, $V_G = 5.7$ μ/s) and BB-W (proportional to ground displacement, $T_u = 60$ s, $V_{max} = 1{,}750$) and simulated seismograms of the systems KIRNOS ($V_{max} = 2{,}500$), GALITZIN ($V_{max} = 3{,}000$), WWSSN-LP ($V_{max} = 3{,}000$) and WWSSN-SP ($V_{max} = 25{,}000$) of a deep focus earthquake in the North Korea region on March 9, 1977 (14 h 27 m 53.6 s, 41.6 °N, 130.9 °E, $h = 528$ km, $m_b = 5.9$, $\Delta = 74.8°$). Instrument parameters in Table 1

instruments is the calculation of equivalent Wood-Anderson amplitudes by point-by-point amplitude conversion. The transformation of short period records into synthetic Wood-Anderson seismograms by Fourier transform was described by Bakun et al. (1978). In the routine seismogram analysis at the Seismological Observatory Graefenberg M_L is calculated by simulating a Wood-Anderson seismograph in the time domain with a two-step recursion filter corresponding to Eqs. (15) and (16).

The transfer function $H_{WA}(\dot{s})$ of a continuous filter which transforms the broad-band seismogram u into the simulated seismogram x of a Wood-Anderson seismograph is given, in analogy to Eq. (1) by

$$H_{WA}(s) = H_0^{-1}(s) \cdot H_3(s) \tag{17}$$

$H_0^{-1}(s)$ is the inverse transfer function of the broad-band seismograph in Eq. (2) and

$$H_3(s) = V_3 \frac{s^2}{s^2 + 2h_3\omega_3 s + \omega_3^2} \tag{18}$$

is the transfer function of the Wood-Anderson seismograph (displacement transducer with the natural period $T_3 = 0.8$ s, damping constant $h_3 = 0.8$ and magnification $V_3 = 2{,}800$). From Eqs. (2), (17), and (18), and omitting the gain factor V_3 it follows

$$H_{WA}(s) = \frac{s^2 + 2h_0\omega_0 s + \omega_0^2}{s^2 + 2h_3\omega_3 s + \omega_3^2} \cdot \frac{1}{s}. \tag{19}$$

Application of the z-form method to Eq. (19) enables the simulation of a Wood-Anderson seismograph as a two-step recursion filter in the time domain in analogy to Eqs. (6) to (16):

$$v_t = f_0 u_t + f_1 u_{t-1} + f_2 u_{t-2} - g_1 v_{t-1} - g_2 v_{t-2} \tag{20}$$

$$x_t = h_0(v_t + v_{t-1}) + x_{t-1}. \tag{21}$$

The filter coefficients f_i and g_i are given by the coefficients a_i and b_i in Eq. (9) when ω_3' takes the place of ω_1' from Eq. (6) and k_1' is replaces by $k_3' = 2h_3\omega_3'$.

The recursion Eq. (21) which is derived from the factor 1/s in Eq. (19) corresponds to the trapezoidal rule for numerical integration with $h_0 = \Delta t/2$.

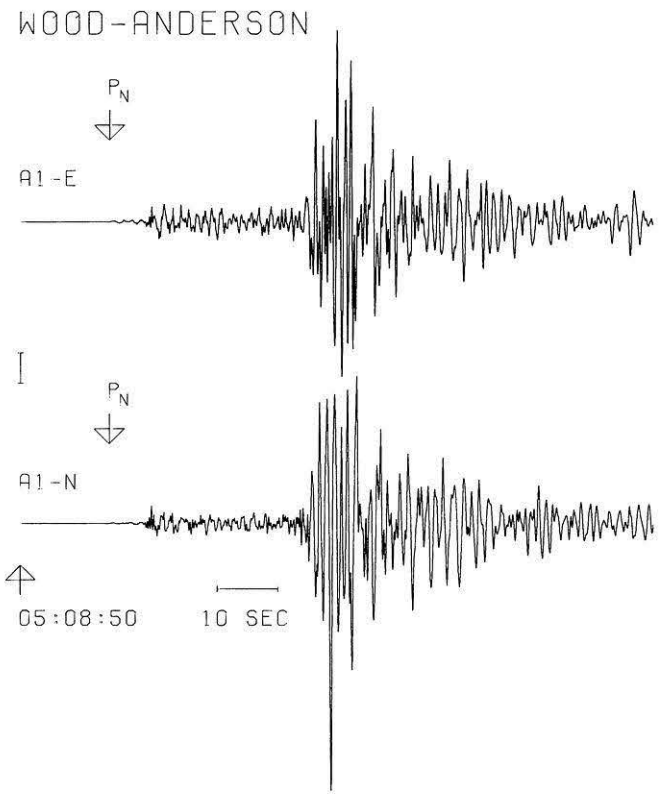

Fig. 8. Simulated Wood-Anderson seismograms of the Albstadt earthquake on September 03, 1978 (05 h 08 m 31.8 s, 48.28 °N, 9.03 °E, $h = 6.6$ km, $M_L = 5.9$, $\Delta = 224$ km) $V_{max} = 1{,}000$ related to marked amplitude scale of 1 cm

The Graefenberg-array, which was designed to record teleseismic signals has a frequency cut-off at 5.0 Hz determined by the anti-aliasing filter of the data acquisition system. Thus systematic errors can occur in the determination of M_L for near earthquakes with small epicenter distances. The seismic active area nearest to the Graefenberg-array is the Swabian Jura (mean distance about 200 km). The M_L values calculated with the Wood-Anderson simulation filter from Graefenberg broad-band recordings are generally in very good agreement with the local magnitudes derived from analog seismograms of the Swabian Jura station network (recording proportional to ground displacement between the 3-db periods 1.5 s and 50 s).

As an example Fig. 8 shows the simulated Wood-Anderson seismograms for the Albstadt earthquake on September 3, 1978. M_L was determined to be $M_L = 5.9$.

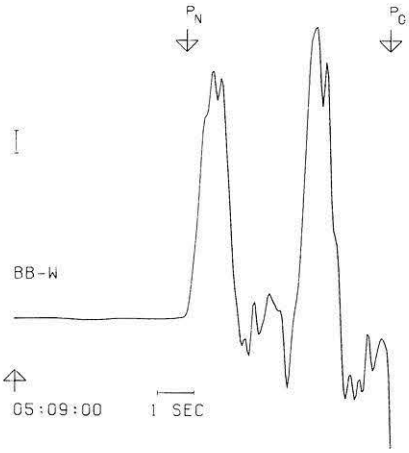

Fig. 9. Broad-band recording BB-W (proportional to ground displacement, $T_u = 22.5$ s, $V_{max} = 15{,}000$) of P_n-wave for the same earthquake as in Fig. 8

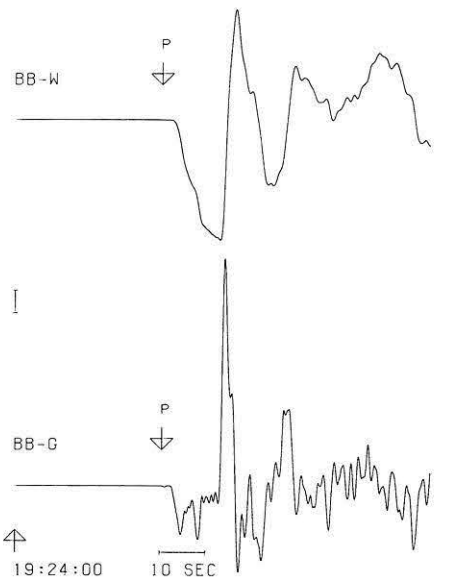

Fig. 10. Broad-band recording BB-W (proportional to ground displacement, $T_u = 172$ s, $V_{max} = 100$) and BB-G (proportional to ground velocity, $T_u = 200$ s, $V_G = 59$ μ/s) of P-wave for the same earthquake as in Fig. 5

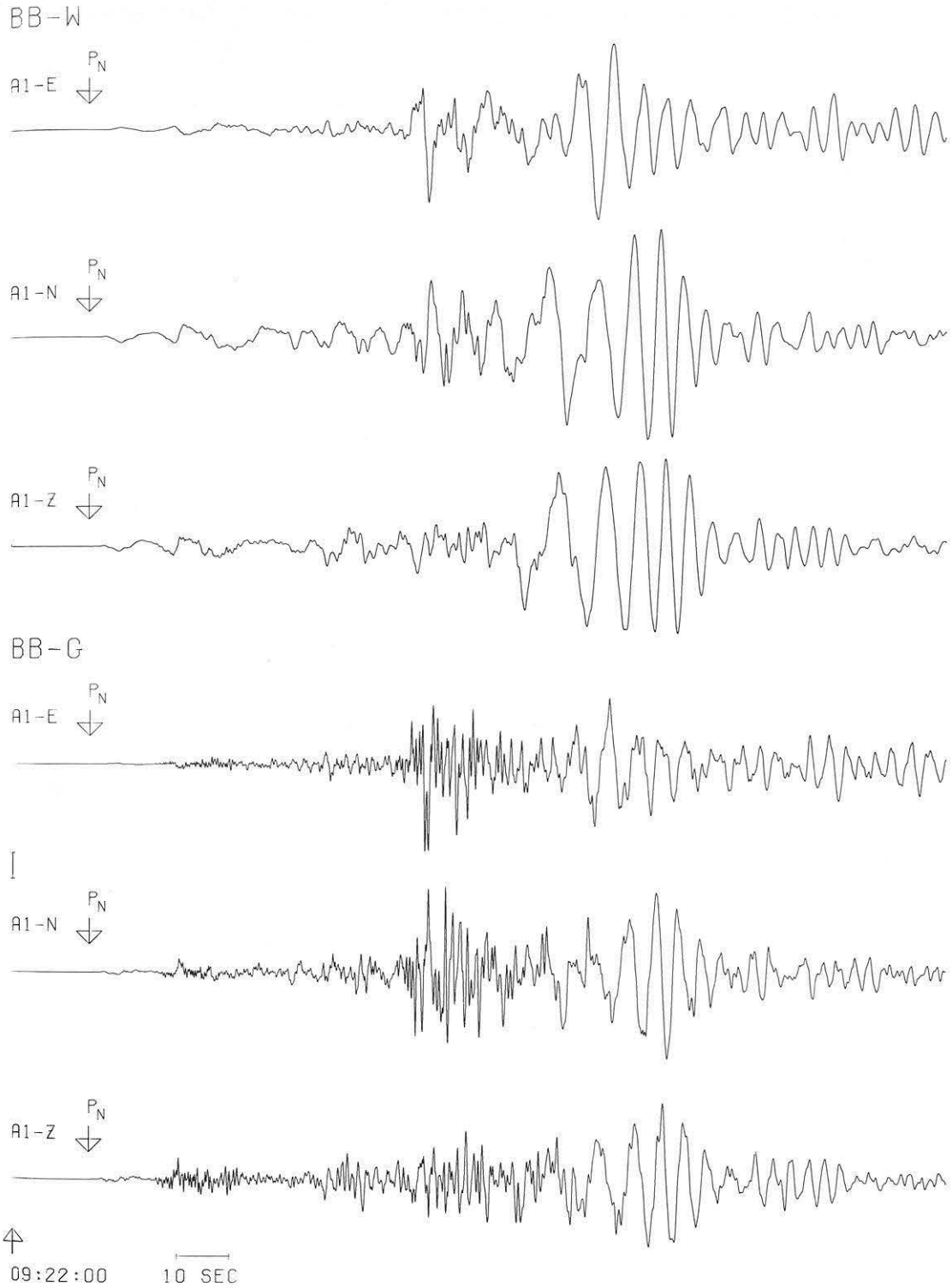

Fig. 11. 3-component recording BB-W (proportional to ground displacement, $T_u = 22.5$ s, $V_{max} = 50$) and BB-G (proportional to ground velocity, $T_u = 30$ s, $V_G = 367$ μ/s) of a Friuli earthquake on September 15, 1976 (09 h 21 m 19.1 s, 46.3 °N, 13.1 °E, $m_b = 5.4$, $\Delta = 3.6°$)

Restitution by Simulation

The restitution or restoration problem is the problem of reconstructing the input signal from the output signal of a band-limited system with a known transfer function.

The formal solution of this problem results from multiplication of the spectrum of the output signal with the inverse system transfer function and transformation to the time domain. Since the inverse transfer functions of seismograph systems with displacement or velocity transducer have a pole of second

or third order at $s=0$, the restitution problem in seismology, that is, the determination of the true ground motion in terms of displacement, velocity or acceleration, can only be solved approximately by shifting the pole to the left s-half plane. The accuracy of the approximation is determined less by the mathematical method than by the quality of the data (spectrum of the input signal, bandwidth, linearity, dynamic range, resolution and low-frequency instrument noise of the entire seismograph and recording system). A comparison of various methods (J. Geophys. 39, 501–626, 1973) has shown that a numerical restitution of digitized narrow-band analog seismograms usually does not produce useful results. In principal, the restitution of digitized broad-band seismograms has the same limitations, but better data quality allows sufficient accuracy for practical purposes (for example determination of seismic moment). A summary of various restitution methods in the time and frequency domain can be found in the above mentioned special issue 'Seminar on deconvolution of seismograms and high-fidelity seismometry' (J. Geophys. 39, 501–626, 1973).

Since the parameters for a seismometer-galvanometer system can always be chosen so that the transfer function is proportional to ground displacement, velocity or acceleration in a specified frequency range the restitution problem can also be solved by the simulation of an appropriately chosen seismometer-galvanometer combination.

The parameters (T_1,h_1, and T_2, h_2, natural period and damping constant of seismometer and galvanometer, respectively) of a seismometer-galvanometer system whose transfer function is proportional to ground displacement, velocity or acceleration in the period interval $T_A < T < T_B$ can be deduced from the following approximation formulas (Savarenski and Kirnos 1960):

Displacement

$$T_1 \gg T_B \quad h_1 = 0.4 \quad T_2 = \sqrt{T_A T_B} \quad h_2 \gg 1$$

Velocity

$$T_1 \gg T_B \quad h_1 = 0.4 \quad T_2 \ll T_A \quad h_2 \leqq 1.$$

Acceleration

$$T_1 \ll T_A \quad h_1 < 1 \quad T_2 = \sqrt{T_A T_B} \quad h_2 \gg 1.$$

In the above equations, the seismometer and galvanometer parameters can be interchanged.

An example of a displacement proportional system is given by the KIRNOS characteristic in Table 1. For the simulation filter, the upper 3-db period T_u can be raised to a maximum value determined only by the low-frequency signal to noise ratio. The maximum value for a specific seismogram is best determined by systematically raising T_u until the limit of the stable region is reached.

Using as an example the parameters

$$T_1 = 100\,\text{s}, h_1 = 0.4, \quad T_2 = 2\,\text{s}, h_2 = 10.0$$

one gets $T_u = 58$ s as an upper 3 db-period, whereas for

$$T_1 = 180\,\text{s}, h_1 = 0.5, \quad T_2 = 10\,\text{s}, h_2 = 8.0$$

this upper bound is $T_u = 172$ s.

A seismometer-galvanometer system with broad-band velocity recording is described in Table 1 by the long-period BENIOFF-LP characteristic. The velocity proportional seismograms BB-G in Figs. 3–11 were calculated from broad-band Graefenberg recordings through digital inverse filtering using Eq. (15). A seismometer-galvanometer system recording proportional to ground acceleration between the 3 db-periods $T_l = 0.08$ s and $T_u = 40$ s can be realised for example with the parameters $T_1 = 0.05$ s, $h_1 = 0.5$, $T_2 = 2.0$ s, $h_2 = 10.0$.

An important application of the restitution problem is the calculation of the displacement – time integral of the *P*-wave to determine the seismic moment. Figure 9 shows the displacement proportional seismogram of the P_n-wave group for the Albstadt earthquake on September 3, 1978. The first half-oscillation gives a value of $6.3\ 10^{-6}$ m s. Figures 10 and 11 show the restituted displacement and velocity proportional seismograms of the *P*-wave for the Bukarest earthquake on March 4, 1977, and a 3-component recording of the Friuli earthquake on September 15, 1976.

Acknowledgements. I thank H.-P. Harjes for many valuable and stimulating discussions and Mrs. M. Hellweg for translating the manuscript. I am greatly indebted to C. Kisslinger for critically reading the manuscript and for several helpful suggestions. The GRF-array project is supported by the Deutsche Forschungsgemeinschaft (German Research Council) and the Bundesanstalt für Geowissenschaften und Rohstoffe (Federal Institute for Geosciences and Natural Resources).

References

Bakun, W.H., Houck, S.T., Lee, W.H.K.: A direct comparison of synthetic and actual Wood-Anderson seismograms. Bull. Seismol. Soc. Am. **68**, 1199–1202, 1978

Beauchamp, K.G.: Signal processing. London: George Allen & Unwin LTD 1973

Chakrabarty, S.K., Choudhury, G.C., Roy Choudhery, S.N.: Magnification curves of electromagnetic seismographs. Bull. Seismol. Soc. Am. **54**, 1459–1471, 1964

Harjes, H.-P., Seidl, D.: Digital recording and analysis of broadband seismic data at the Graefenberg (GRF)-array. J. Geophys. **44**, 511–523, 1978

Kaiser, J.F.: Design methods for sampled data filters. Proc. 1st Annu. Allerton Conf. Circuit System Theory pp. 221–236, 1963

Kind, R.: Observations of sPn from Swabian Alb earthquakes at the GRF array. J. Geophys. **45**, 337–340, 1979

Müller, G., Bonjer, K.-P., Stöckl, H., Enescu, D.: The Romanian earthquake of March 4, 1977. I. Rupture process inferred from fault-plane solution and multiple-event analysis. J. Geophys. **44**, 203–218, 1978

Peterson, J., Butler, H.M., Holcomb, L.G., Hutt, C.R.: The Seismic Research Observatory. Bull. Seismol. Soc. Am. **66**, 2049–2068, 1976

Savarenski, E.F., Kirnos, D.P.: Elemente der Seismologie und Seismometrie. Berlin: Akademie-Verlag 1960

Savill, R.A., Carpenter, E.W., Wright, J.K.: The derivation and solution of indicator equations for seismometer-galvanometer combinations including the effect of seismometer inductance. Geophys. J. R. Atron. Soc. **6**, 409–425, 1962

Stoll, D.: Spektralanalyse seismischer Wellen zur Beschreibung des Scherbruches bei den Erdbeben in Friaul (1976), 48 pp. Diplomarbeit, Universität Stuttgart 1979

Streckeisen, G.: Wide-band feedback seismograph system STS-1V/STS-1H. Prospekt der Firma G. Streckeisen

Meßgerätebau, Buchsweg 17, CH-8400 Winthertur, Schweiz 1978
Wielandt, E.: Ein einfacher elektronischer Entzerrer für Seismometer. J. Geophys. **36**, 763–769, 1970
Wielandt, E.: Noise in electronic seismograph systems. J. Geophys. **39**, 597–602, 1973
Wielandt, E.: Ein astasiertes Vertikalpendel mit tragender Blattfeder. J. Geophys. **41**, 545–547, 1975
Wielandt, E., Mitronovas, W.: An electronic long-period seismograph for surface-wave dispersion studies. Bull. Seismol. Soc. Am. **66**, 987–996, 1976
Willmore, P.L., Karnik, V.: Manual of seismological observatory practice. International Seismological Centre Edinburgh, Scotland 1970
Proceedings. Seminar on deconvolution of seismograms and high-fidelity seismometry. J. Geophys. **39**, 501–626, 1973

Received June 22, 1979; Revised Version February 15, 1980